Red- to NIR-Emitting, BODIPY-Based, K^+-Selective Fluoroionophores and Sensing Materials

Bernhard J. Müller, Sergey M. Borisov, and Ingo Klimant*

Optical sensing materials for the selective measurement of potassium ions (K^+) in water are presented. The indicator dyes are based on an aza-crown ether as a receptor and borondipyrromethenes (BODIPY) dyes as fluorophores. Fluorescence enhancement is caused by the reduction of photoinduced electron transfer (PET) upon complexation with K^+ ions. The family of new indicators possesses tuneable optical properties (green to red excitation, red to NIR emission) and PET efficiencies. They exhibit high brightness with quantum yields between 0.20 and 0.47 in the "on" state and a molar absorption coefficient between 30 000 and 290 000 M^{-1} cm^{-1}. The new indicator dyes are immobilized in biocompatible hydrogel matrices to obtain stable nonleaching and fast responding ($t_{90} \approx 10$ s) sensing materials for continuous measurements of potassium. They are realized in various formats such as planar optodes, fiber-optic sensors, and water-dispersible polymer-based nanoparticles. Apart from fluorescence intensity measurements, self-referenced read-out of fluorescence decay time is demonstrated. All sensor materials display a high K^+/Na^+ selectivity and are not influenced by pH within the physiologically relevant range. Practical applicability of the materials is emphasized by application of a fiber-optic sensor to quantification of K^+ in serum, which shows excellent correlation with the reference measurements.

1. Introduction

Potassium (K^+) plays a central role in the human body and is necessary for the function of all living cells. Inside the cell K^+ is the main ion with an approximate concentration of 150×10^{-3} M while extracellular concentrations are about 5×10^{-3} M.[1,2] The difference in concentration causes a disparity in electric potential between the interior and exterior of cells, known as the membrane potential.[3] It takes part in substantive processes and functions such as the regulation of cell growth, acid-base equilibrium, and maintaining the normal blood pressure.[4–6] Cells can control this potential by opening or blocking K^+ channel transmembrane proteins.[7] This regulation of intra- and extracellular K^+ concentration plays a key role in metabolic processes and is of high interest for pharmacological research. However, the molecular mechanism of potassium physiology and pathology are still insufficiently understood, partly due to the lack of tools for measuring K^+.

B. J. Müller, Dr. S. M. Borisov, Prof. I. Klimant
Institute of Analytical Chemistry and Food Chemistry
Graz University of Technology
Stremayrgasse 9, 8010 Graz, Austria
E-mail: sergey.borisov@tugraz.at

DOI: 10.1002/adfm.201603822

Extracellular potassium (whole blood, serum) is the key analyte in clinical diagnostics as elevated K^+ concentration (hyperkalemia) is an indication for cardiac arrhythmia which can lead to sudden heart failure.[8] The crucial requirement and greatest challenge for potassium sensors for clinical diagnostics is the selective detection of the low extracellular K^+ (5×10^{-3} M) over a high Na^+ concentration (150×10^{-3} M).[9] Apart from good selectivity, inertness to variations of pH in the relevant range is of extreme importance.

Fluorescence-based measurements offer several advantages compared to other analytical techniques (e.g., electrochemical measurements with ion selective electrodes) as they are free of electromagnetic interferences and are noninvasive. Fluorescent sensors are available in various formats including planar sensors and spots, fiber-optic sensors and (nano)particles. Nanoscale sensing materials can be incorporated into small objects such as cells to gain information in real time or enable high-resolution imaging.[10] Conventional fluorescence and laser-scanning microscopes can be used for this purpose.[11,12]

A fluorescent indicator dye typically consists of a fluorophore linked to a recognition unit (receptor/ionophore) leading to a fluoroionophore. Fluoroionophores based on intramolecular quenching due to photoinduced electron transfer (PET) have been applied successfully for sensing cations in the last years.[13] Typically, the receptor unit bears a tertiary amine group which is responsible for the emission enhancement in presence of ions, due to the reduction of the PET effect.

PBFI (potassium binding benzofuran isophthalate) consisting of a diaza-18-crown-6 ether as a receptor and a benzofuran derivative as a fluorophore is the most popular indicator dye for molecular biology studies and the only commercially available fluoroionophore.[14] However, this PBFI indicator suffers from a poor K^+/Na^+ selectivity and is expensive. A triazacryptand (TAC) receptor designed by He et al.[15] shows excellent K^+ selectivity and sensitivity, but its preparation is very tedious due to extensive multistep synthesis. Hence, there is a high demand for simple, sensitive, and selective receptors.

Recently, Ast et al. introduced a phenylaza-[18]crown-6 with ortho-substituted 2-methoxyethoxy group as receptor which has a good K^+/Na^+ selectivity and is simpler to prepare than the TAC receptor.[16] Combining this receptor with a

coumarin fluorophore enabled measurement of K^+ in the range of 2×10^{-3}–100×10^{-3} M with a negligible cross-sensitivity to Na^+ under physiological conditions and a 2.5-fold fluorescence enhancement at 160×10^{-3} M K^+ at 493 nm. The fluorophores used for optical K^+ sensing included derivates of coumarins,[16] xanthene dyes,[17–19] naphthalimides,[15,20] borondipyrromethenes (BODIPYs),[21–26] and other dyes.[27] Most of them are excitable below 600 nm (Table S1, Supporting Information). However, indicator dyes with longer wavelength of absorption and emission (>600 nm) are of particular interest as they allow measurements in highly scattering and absorbing media (e.g., tissues) as well as in autofluorescent media (e.g., biological samples).

The fluoroionophores for intracellular imaging of K^+ reported by the groups of Verkman and Meldrum were modified with charged groups in order to facilitate the solubility in water and to enable cell uptake. Application of such probes is limited to assays in small volumes (such as cells) since they have to be added to the analyzed media. Thus, immobilization of the fluoroionophores into polymeric matrices is necessary to design sensors for continuous monitoring of the analytes (e.g., in diagnostics). Despite seemingly straightforward, this can be a challenging task since (i) it should be ensured that the material possesses good permeability for the analyte, i.e., is sufficiently hydrophilic; (ii) the indicator should be compatible to the matrix to prevent aggregation; (iii) it should not leach out of the matrix which is not unlikely for the dyes bearing hydrophilic receptors. Last but not least, not all indicators which work properly in solution show a response when immobilized in a hydrogel, as the environmental polarity plays an important role in the PET effect. In fact, very few sensors based on immobilized indicators have been reported so far.[15,16,20] They employed fluoroionophores which show excitation and emission at shorter wavelength and only moderate brightness. Thus, preparation of novel high performance sensing materials for K^+ remains of utmost importance.

In this contribution we report a palette of K^+ fluoroionophores based on BODIPY dyes having tuneable spectral properties, good brightness, insensitivity to pH in the relevant conditions and tuneable sensitivities. They incorporate a selective, yet conveniently accessible aza-crown-ether receptor. We will report on preparation and properties of novel materials (solid state optical sensors and potassium-sensitive nanoparticles) which enable numerous applications in science and technology exemplary demonstrated for measurement in fetal bovine serum samples.

2. Results and Discussion

2.1. Synthesis of BODIPY Fluoroionophores

The new fluoroionophores (**FIs**) represent a highly modular system consisting of two building blocks—the receptor and the chromophore (**Figure 1**). The spectral properties are controlled by the pyrroles and the sensitivity is controlled by the receptor which enables high flexibility of the design. The synthesis of the receptor (o-(2-methoxyethoxy)phenylaza-[18]crown-6 lariat ether) was performed as described by Ast et al.[16] (Figure S1, Supporting Information). Importantly, this convenient procedure relies on readily available reagents and allows preparation of multigram quantities of the receptor. All the BODIPY indicators are prepared via condensation of a pyrrole and the aromatic aldehyde from the receptor, subsequent oxidation with DDQ and complexation using a base and BF_3–etherate. We prepared differently substituted pyrroles in order to tune the optical properties and optimize the PET efficiencies of the indicators (**Figure 2**). Whereas 2,4-dimethylpyrrol is commercially available, other pyrrols can be conveniently prepared from the respective ketones and 3-phenyl-2H-azirene.[28] A different route is necessary for preparation of furan-fused pyrrols.[29]

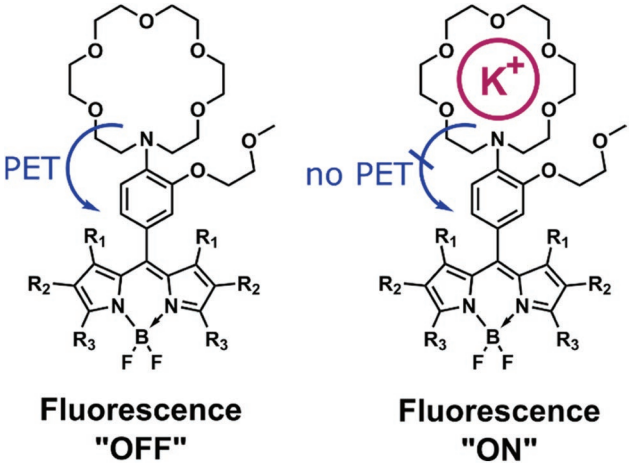

Figure 1. Operating principle of a fluorescent K^+ probe. Fluorescence enhancement is caused by complexation of K^+ and a reduction of the photoinduced electron transfer (PET).

2.2. Spectral and Electrochemical Properties of the New Fluoroionophores

FI 1 prepared from 2,4-dimethylpyrrol is a commonly used BODIPY dye with absorption in the blue and emission in the green region of the electromagnetic spectrum (**Figure 3** and **Table 1**). A bathochromic shift of about 70 nm is obtained via extension of the aromatic system to tetraphenyl-BODIPY **FI 2**. Rigidization results in an even further bathochromic shift of the absorption and emission (about 70 nm), higher molar absorption coefficients and fluorescence quantum yields (Table 1). As expected **FI 4** absorbs at longer wavelength compared to **FI 3** due to the electron-donating character of the methoxy-group. **FI 3** and **FI 4** can be efficiently excited using red light and show emission in the red/NIR part of the spectrum. **FI 5** includes a fused furan ring and belongs to the so-called Keio Fluors variation of BODIPYs.[30] This dye class has extraordinarily high molar absorption coefficients and high quantum yields. Indeed, the indicator FI 5 demonstrates ε of 195 600 M^{-1} cm^{-1} and QY of 60% in the "on" state (Table 1). BODIPY indicators are well known for their sharp and narrow absorption and emission spectra[31] which is also the case for all new fluoroionophores except **FI 2**. It shows a very broad absorption and consequently a lower molar absorption coefficient. This can be attributed to the rotation of the phenyl

Adv. Funct. Mater. 2016,
DOI: 10.1002/adfm.201603822

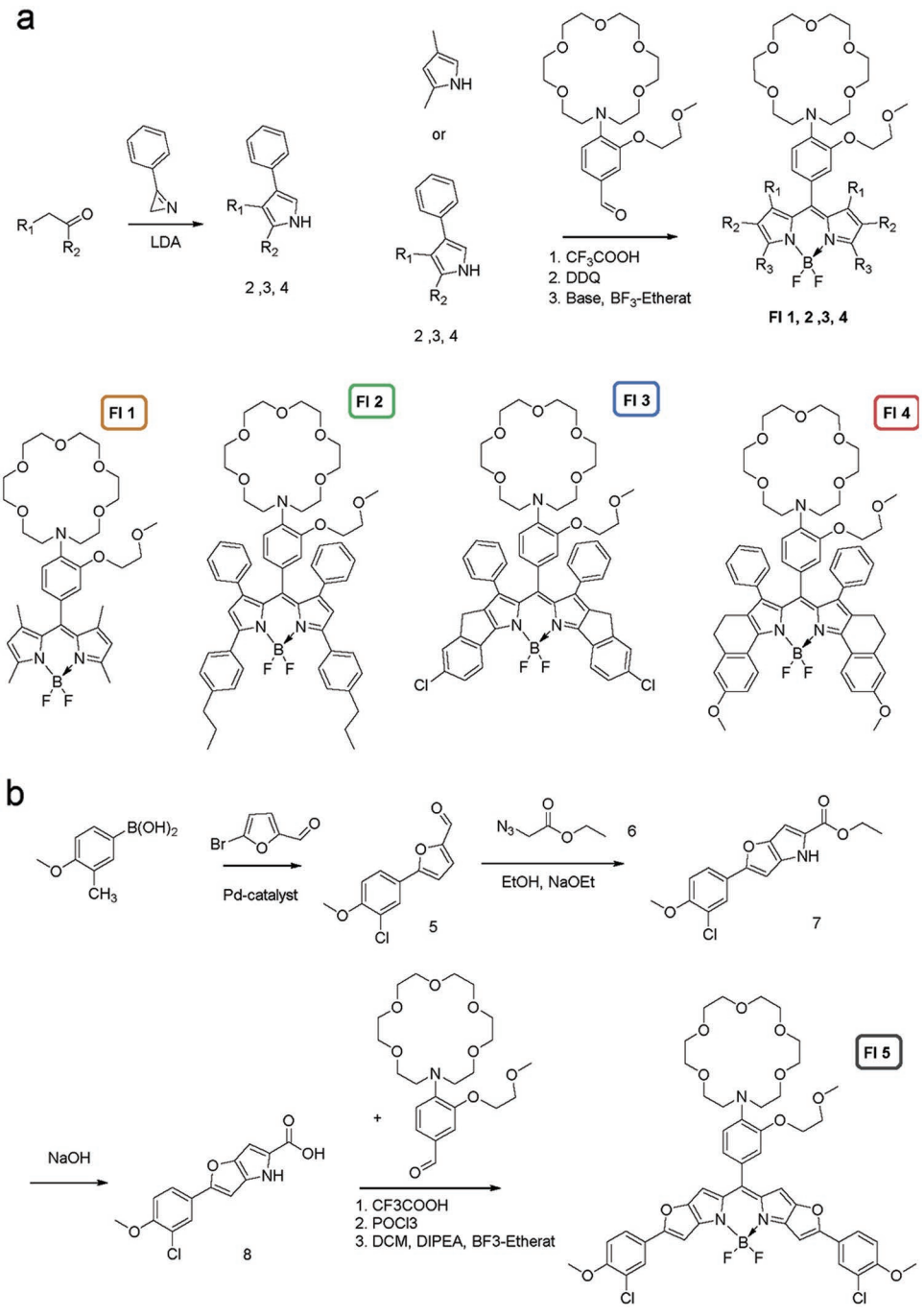

Figure 2. a) Synthesis of different pyrroles and BODIPY indicators. b) Synthetic pathway to FI 5.

rings, since aggregation of the dye was not observed. **FI 2** already shows an appreciable quantum yield of 35% in solution when protonated with trifluoracetic acid whereas the quantum yields for BODIPYs **FI 1**, **3**, **4**, and **5** in solution are significantly higher. Luminescence lifetimes in the "on"-state (fully protonated) vary from 3.1 to 5.1 ns. To conclude, all the new fluoroionophores feature excellent fluorescence brightness (BS) which is particularly high for **FI 5**.

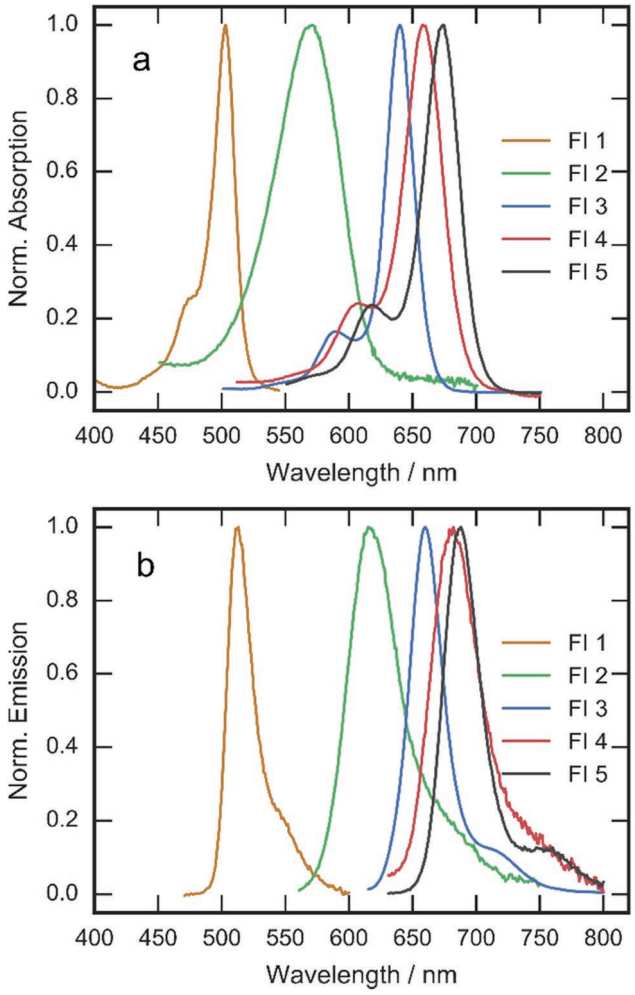

Figure 3. a) Normalized absorption and b) emission spectra of the fluoroionophores in dichloromethane.

Cyclovoltammetric measurements (Figure S2, Supporting Information, and Table 1) show that **FI 2** and **FI 3** are more difficult to oxidize than **FI 4** and **FI 5** which indicates more electron-rich character of the latter. **FI 1** bearing 4 electron-donating methyl groups instead of electron-withdrawing aryls shows significantly lower oxidation potential compared to other **FIs**. The trend in the ground state reduction potentials is less evident. However, the reduction potentials estimated for the excited state ($E_{1/2}$red*) from the reduction potential in the ground state ($E_{1/2}$red) and the energy of the excited state (E_{00}) clearly show that **FI 1–3** in the excited state are more powerful oxidants than **FI 4** and **FI 5**. In the same conditions, the oxidation potential of the free aza-crown receptor ($E_{1/2}$ox(rec)) was estimated to be 0.817 V. Thus, ΔG of the electron transfer reaction (ΔG_{PET} = $E_{1/2}$ox(rec)–$E_{1/2}$red*(FI)[32]) is negative for **FI 1–FI 3** but close to zero for **FI 4** and **FI 5**. An increase in $E_{1/2}$ox(rec) by at least 0.1 V is detectable in presence of K^+ (Figure S2g, Supporting Information) indicating the increase in ΔG of quenching reaction. It should be mentioned that the absolute values are just a very rough estimation due to the fact that the ion pairing energy describing charge generation and separation within the electron-transfer complex is neglected and E_{00} was estimated from fluorescence maxima and not on the edge of the spectra.

2.3. Polymer-Based Sensing Materials

In order to prepare solid state sensing materials the fluoroionophores have to be immobilized in a hydrogel matrix (**Figure 4**). This was achieved by simply dissolving the dyes and the polymer in organic solvent and coating the resulting "cocktail" onto a transparent inert polyethylene terephthalate support. Hydromed D4 was chosen as a suitable matrix due to its capability to take up about 100% water, good ion permeability, biocompatibility, and commercial availability. As can be seen from Figure 4 immobilized **FI 1** leaches continuously out of the sensor matrix into the analyzed solution. Leaching of the dye can be attributed to very hydrophilic nature of the receptor which is particularly pronounced in presence of K^+ due to the charged nature of the resulting complex. In contrast to **FI 1**, indicators **FI 2–5** are significantly more hydrophobic which completely eliminates leaching (Figure 4 and Figure S3, Supporting Information). Due to instability of **FI 1**-based sensors only materials based on **FI 2–5** were characterized. The calibration curves for the sensors were obtained in 20×10^{-3} M TRIS buffer at pH of 7.4 (representing the pH of blood) with different KCl concentrations (**Figure 5**). As can be seen, the fluorescence intensity greatly increases in presence of the analyte due to decreased efficiency of PET from the amino group of the receptor to the chromophore. For **FI 2** and **FI 3** the relative fluorescence enhancement in presence of K^+ is higher than for **FI 4** and **5**. This behavior is attributed to the electron-donating effect

Table 1. Photophysical and electrochemical properties of the fluoroionophores in solutions and immobilized in a hydrogel matrix (D4).

Dye	λmax abs (ε) [nm] ([M^{-1} cm^{-1}])	λmax em [nm]	QY in THF[a)]	BS, ε·QY	QY in D4 with 1 M KCl	QY in D4 with 0.1 M HCl	Lifetime in THF[a)] [ns]	$E_{1/2}$ ox [V]	$E_{1/2}$ red [V]	$E_{1/2}$ ox*[b)] [V]	$E_{1/2}$ red*[c)] [V]
FI 1	504 (53 600)	513	0.66	35 376	n.d.	n.d.	5.1	0.44	–1.27	–1.98	1.15
FI 2	571 (29 900)	615	0.35	10 465	0.20	0.64	3.5	0.93	–0.95	–1.09	1.07
FI 3	640 (109 300)	660	0.68	74 324	0.47	0.76	5.0	1.08	–0.82	–0.80	1.06
FI 4	655 (87 200)	682	0.53	46 216	0.47	0.46	4.1	0.80	–1.03	–1.02	0.79
FI 5	670 (195 600)	688	0.60	117 360	0.42	0.41	3.1	0.88	–0.88	–0.92	0.92

[a)]Contains 3% v/v trifluoroacetic acid; [b)]Calculated as $E_{1/2}$ ox* = $E_{1/2}$ ox – E_{00}; E_{00} is estimated from the λmax em; [c)]Calculated as $E_{1/2}$ red* = $E_{1/2}$ red + E_{00}; E_{00} is estimated from the λmax em.

Adv. Funct. Mater. **2016**,
DOI: 10.1002/adfm.201603822

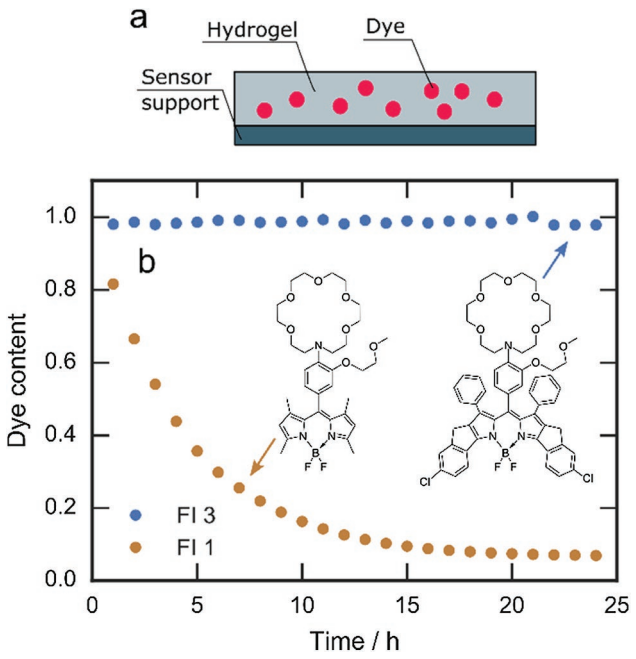

Figure 4. a) Scheme of a polymer-based sensing material. The fluoroionophores are physically immobilized in a polymer hydrogel matrix. b) Normalized absorption maxima of the fluoroionophores immobilized in hydrogel D4. 100×10^{-3} M KCl solution was pumped through a flow-through cell for 24 h.

of the methoxy groups in both indicators (**FI 4** and **5**) which decrease the PET efficiency in the absence of K^+. Therefore, these fluoroionophors show emission in the absence of K^+ whereas the emission of **FI 2** and **3** is "switched off" almost completely in the same conditions (Figure 5c,f and Figure S4b,d, Supporting Information). This findings show good correlation with the results of the electrochemical investigation.

The emission spectra (Figure 5) show only a minor bathochromic shift in presence of K^+ and upon protonation of the receptor in acidic media, which indicates that the PET effect is predominant over intramolecular charge transfer (ICT).

Comparison of the very similar rigid chromophores **FI 3** and **FI 4** reveals that systematic tuning of the PET efficiency is easily possible. Significant increase in the dynamics for **FI 4** and **FI 5** is expected if further electron-withdrawing substituents (halogens, sulphonamides) are introduced into the chromophore. The normalized F/F_0 values at 5×10^{-3} M K^+ (typical extracellular concentration), 150×10^{-3} M K^+ (typical intracellular concentration), and at saturation of the sensor (1 M K^+) as well as Kd values for each sensing material are listed in **Table 2**. The Kd value of the indicators inside the polymer membrane were determined using the Benesi–Hildebrand equation as described in literature[27] (Equation (S1), Supporting Information). Almost ideal linear fit (Figure 5e,f) indicates a 1:1 complexation behavior. K_d can be calculated using the slope of the fit. The relative fluorescence enhancement in case of **FI 2** and **3** is very good at low K^+ concentrations and the

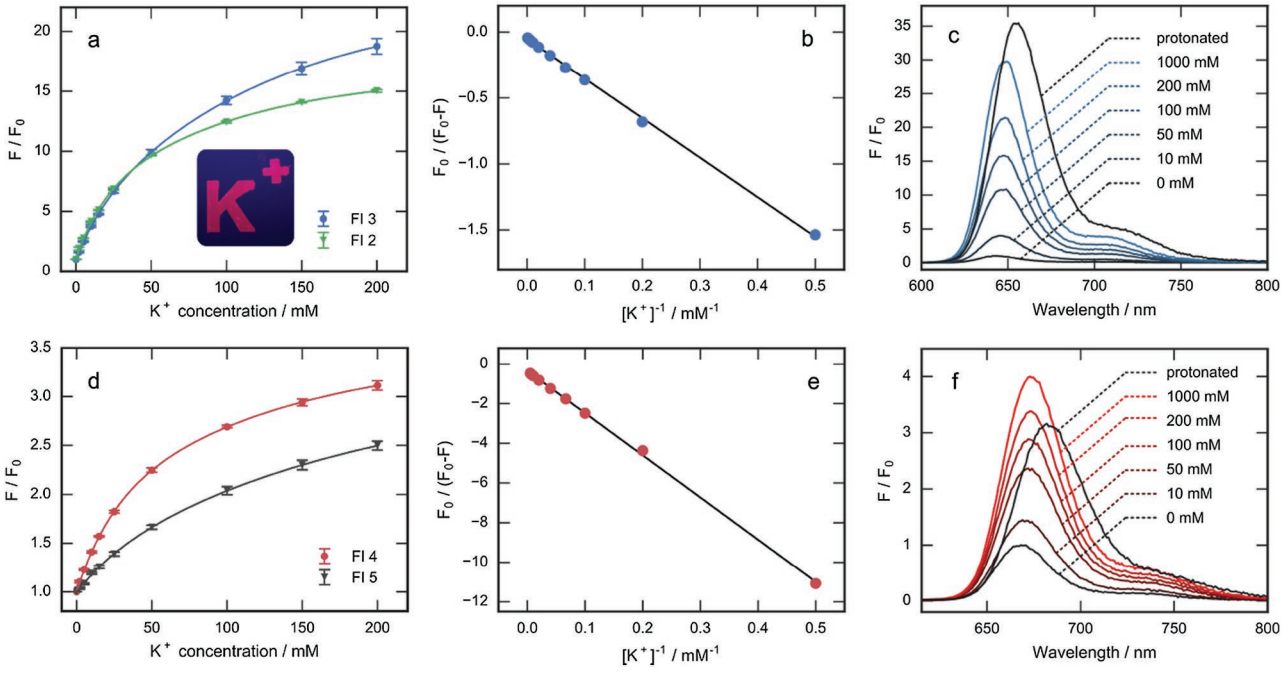

Figure 5. a,d) F/F_0 calibration curves for **FI 2–5** immobilized in hydrogel D4. The values of F and F_0 were taken at λ = 605, 645, 668, and 685 nm for FI 2, FI 3, FI 4, and FI 5, respectively. b,e) Exemplar Benesi–Hildebrand plot for **FI 3** and **FI 4** for the determination of Kd via the slope. Benesi–Hildebrand plots for **FI 2** and **FI 5** are shown in the Supporting Information. R^2 of the linear fit is >0.989 for all materials. c,f) Exemplar normalized emission spectra of **FI 3** and **FI 4** with different K^+ concentrations and protonation with 0.1 M HCl. The inset in (a) shows the photographic image (λ_{exc} 365 nm) of hydrogel D4 foil based on **FI 3** with the emission switched on with 150×10^{-3} M K^+.

Table 2. Fluorescence enhancement factors and K_d values for all sensing materials.

Sensor material	F/F_0 at 5×10^{-3} M K^+	F/F_0 at 150×10^{-3} M K^+	F/F_0 at 1 M K^+	K_d [$\times 10^{-3}$ M]
FI 2 in D4	2.8	14.1	18.4	24.1
FI 3 in D4	2.5	16.9	25.5	67.7
FI 4 in D4	1.2	2.9	3.7	37.1
FI 5 in D4	1.0	2.3	3.4	102.7
FI 3 in RL100	1.3	6.7	23.0 (at 800×10^{-3} M)	177.4
FI 3 in PS/PVP	1.7	5.0	11.9	15.6
FI 3 in D4[a)]	2.5	17.5	26.0	66.8

[a)]With 150×10^{-3} M Na^+ background.

dynamic range extends beyond 150×10^{-3} M making these two fluoroionophores promising for both intra- and extracellular measurements.

Since the polymer environment can affect the photophysical properties of the indicators, the QYs of the fluoroionophores in hydrogel D4 were also investigated (Table 1). **FI 2** and **3** show an increased QY in foil when fully protonated (PET off) which can be attributed to a more rigid environment where nonemissive deactivation processes are minimized. However, the QY in 1 M KCl is lower than for the protonated form indicating that K^+ does not fully inhibit the PET effect with these indicators. **FI 4** and **5** have a lower QY in foil than in solution, but the QY of the protonated indicator dyes and the dyes in 1 M K^+ are similar indicating an efficient inhibition of the PET effect by K^+. In general, all indicators show a high QY upon complexation with K^+ in the sensor matrix. Combined with a high molar absorption coefficient this results in very bright sensors. Therefore, indicator dyes can be used for preparation of thin sensor layers which subsequently improves the response time of the sensor.

Since the fluorescence of **FI 4** and **FI 5** is not fully quenched in the absence of K^+ (both free and complexed forms are emissive), self-referenced measurements of the luminescence lifetime become possible (**Figure 6** and Figure S5, Supporting Information). This enables fluorescence lifetime imaging (FLIM) measurements which is of high interest for biological applications.

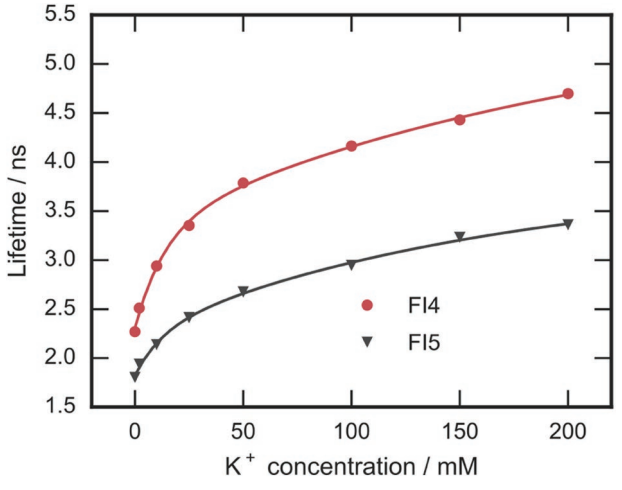

Figure 6. Calibration of **FI 4** and **FI 5** immobilized in hydrogel D4 using fluorescence decay time read-out.

2.4. Selectivity of the Sensor

Inertness to changes of pH in the physiologically relevant range is essential for practical applications of the sensors. As can be seen (**Figure 7**a), the calibration curves are identical at pH 7.1, 7.4, and 7.7. Investigation of the acid–base equilibrium of the aromatic amine of the receptor (**FI 3** in D4) reveals an apparent pK_a value of 3.2 (Figure 7b). Thus, the receptor can be used in the pH range of 5.5–9 without any pH cross-talk, i.e., it is suitable for intra- or extracellular measurements.[33]

FI 3 shows no response to Ca^{2+} or Mg^{2+} (Figure 7c). On the other hand, the indicator dye shows high cross sensitivity to NH_4^+ since the size of NH_4^+ is comparable to that of K^+. However, NH_4^+ does not occur in biological samples in an interfering concentration (except urine) whereas sodium is the main ion present in the extracellular space (150×10^{-3} M). Therefore, the high K^+/Na^+ selectivity of the sensors is of great importance. In fact, **FI 3** shows a fluorescence enhancement of 1.3 at 150×10^{-3} M Na^+ compared to 16.89 at 150×10^{-3} M K^+ and to 2.46 at 5×10^{-3} M K^+. When simulating extracellular conditions (150×10^{-3} M Na^+ background) the F/F_0 and Kd value are only slightly increased compared to 150×10^{-3} M Na^+ background (Table 2). It should be considered that in most applications the concentration of Na^+ does not vary drastically (Figure S6, Supporting Information).

To demonstrate sufficient selectivity over Na^+ ions, we measured the response of a sensor at different K^+ concentrations in presence of 110×10^{-3} and 130×10^{-3} M Na^+. Buffer solutions with different K^+ and Na^+ concentrations were pumped through a flow through cell to imitate extracellular K^+ measurements. **Figure 8** shows that the response of the sensor is fast and fully reversible (a–c). Variation of the Na^+ background from 110×10^{-3} to 130×10^{-3} M at constant K^+ concentration (e–f) does not result is a noticeable cross-talk. Therefore, it is possible to reliably measure K^+ at varying background of Na^+ in the concentration range typical for extracellular measurements. The sensor shows a fast response and recovery (t_{90} = 10 s) and no hysteresis at any concentration. Leaching or aggregation of the dye was not observed either. Interestingly, hydrophobic perylene-based pH indicators previously showed slow response and hysteresis when physically embedded in hydrogel D4.[34] We do not observe such behavior for the potassium fluoroionophores. Therefore, it is likely that the hydrophobic part of the fluoroionophore remains fixed in the hydrophobic domains of the hydrogel whereas much more hydrophilic receptor is localized in the hydrophilic domains.

2.5. Water-Dispersible Nanoparticles

Analyte-sensitive nanoparticles represent versatile analytical tools that are attractive for sensing and imaging in small

Adv. Funct. Mater. **2016**,
DOI: 10.1002/adfm.201603822

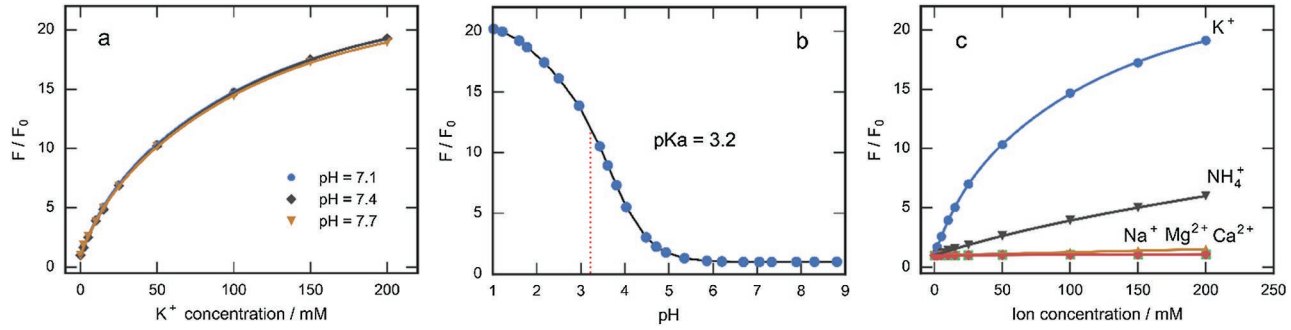

Figure 7. a) Calibration curve for **FI 3** in hydrogel D4 at different pH values. b) Determination of the pKa of the receptor for **FI 3** in hydrogel D4. c) Exemplar determination of the selectivity for FI 3 immobilized in hydrogel D4.

volumes such as cells. Therefore, additionally to planar sensor foils we prepared two different kinds of nanosensors based on commercially available polymers. RL100 is a copolymer of different acrylates with quaternary ammonium groups which are responsible for the excellent cell-penetrating properties of the nanobeads.[35] It is frequently used for drug delivery due to the positive charge and its nonbiodegradability.[36–38] Particles can be prepared in a very simple procedure by dissolving the polymer and the indicator dye in an organic solvent (e.g., acetone) followed by precipitation in water, forming particles with a positive charge outside and the lipophilic indicator entrapped inside.[35,39] The particles show an average size of ≈30 nm and due to the positive charge on the surface the nanoparticle show water uptake and ion permeability.

Figure 9a shows a calibration curve for **FI 3** entrapped in the particles. The sensor material has a higher K_d (177.4×10^{-3} M) compared to hydrogel D4 (67.7×10^{-3} M) which can be attributed to the positive charge of the particles lowering the equilibrium of positively charged K^+ ions inside the particle. Furthermore, the polarity of the polymer is different to Hydrogel D4 affecting the PET efficiency. It should be emphasized that the dynamic range, the spectral properties and the cell penetration of this material match the requirements for intracellular measurements.

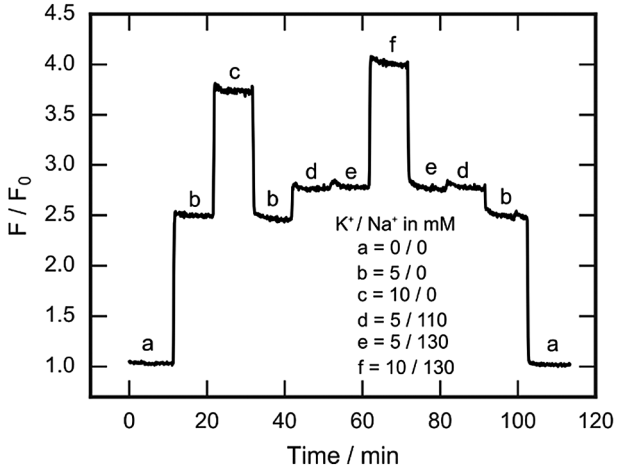

Figure 8. Normalized fluorescence of **FI 3** in hydrogel D4 fixed in a flow-cell while pumping solutions with different K^+ and Na^+ concentrations through it.

Poly(styrene-block-vinylpyrrolidone) (PS/PVP) is a highly versatile particle platform for optical sensors.[40] These commercially-available uncharged particles have an average size of 245 nm and core–shell architecture, which can be used

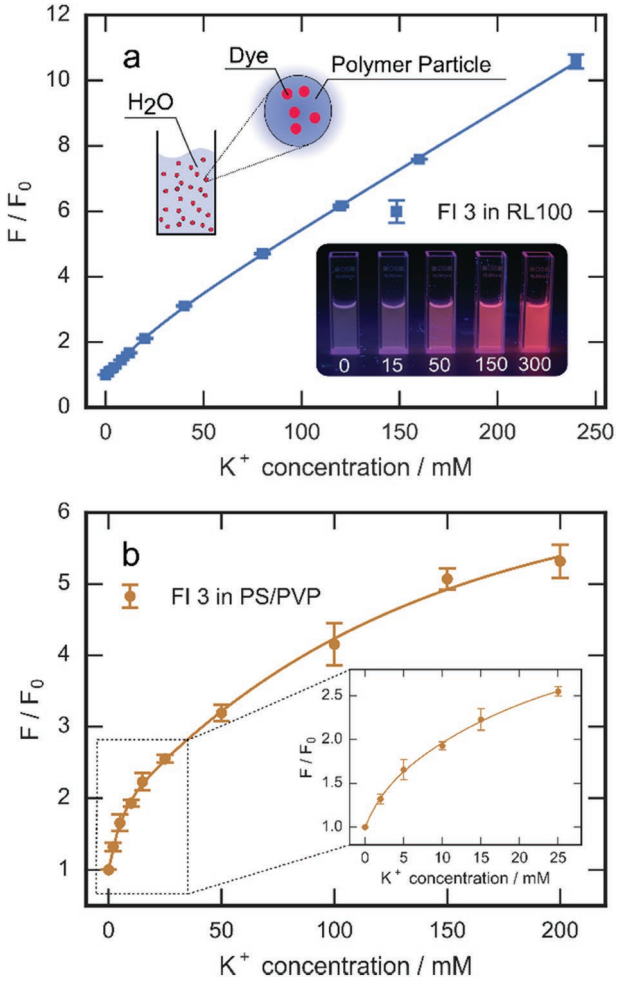

Figure 9. a) Sensing properties of **FI 3** immobilized in positively charged RL100 nanoparticles dispersed in an aqueous solution. The inset shows a photographic image of the aqueous dispersions of the nanoparticles at varying K^+ concentration under 365 nm excitation. b) Sensing properties of PS-PVP nanoparticles stained with **FI 3**. Benesi–Hildebrand plots for both materials are shown in Figure S3 of the Supporting Information.

for incorporation of (indicator) dyes into these two domains. Physical entrapment of the dyes is achieved via swelling the particle with an organic solvent, adding the indicator and then removing the solvent.

We entrapped **FI 3** in the shell in order to allow interaction of the analyte with the indicator. The calibration of the sensor material shows a large dynamic range and a K_d of 15.6×10^{-3} M K^+ (Figure 9b). The most attractive feature of this material is the possibility of incorporating a second dye in the core (e.g., an oxygen indicator for dual sensing or an inert dye for referencing). Also the neutral nature of the particles enhances the sensing options in complex media (e.g., cell cultures) since they do not absorb interfering species, are not incorporated by cells and do not aggregate in samples with high ion concentration.[40]

2.6. Fiber-Optic Sensors

To demonstrate the possible application of the newly developed sensing materials, we fabricated a fiber-optic sensor suitable for read-out with a commercially available phase fluorometer (Firesting, **Figure 10**). In order to ensure a reliable performance the fluorescence intensity of the **FI 3** was referenced against luminescence of Egyptian blue[41] using the so-called dual lifetime referencing (DLR) scheme.[42] Briefly, the overall phase shift is determined only by the ratio of the intensities of the fluoroionophore and the analyte-insensitive long-lived reference luminophore. The sensor material was mounted on the top of an optical fiber using a metal ferrule (Figure 10). Fetal bovine serum (FBS) was used to demonstrate an application of this compact sensor in a complex sample solution. For calibration different FBS samples were prepared by spiking them with KCl solution and determining the real K^+ concentration via ICP-OES since the obtained FBS already contains a certain amount of K^+. The optical sensor shows reproducible performance in serum (Figure 10a). The calibration curve in the low mM range can be fitted linearly ($R^2 = 0.998$, Figure 10b). Three serum samples with unknown K^+ concentration were prepared and measured with the calibrated optode and reference measurements were performed again on ICP-OES. The values obtained with the optodes (21.42×10^{-3}, 23.52×10^{-3}, and 32.59×10^{-3} M K^+ for samples 1, 2, and 3, respectively) showed excellent match with the reference data (21.53×10^{-3}, 23.71×10^{-3}, and 32.27×10^{-3} M, respectively) demonstrating ability of the sensor to accurately measure K^+ concentration in a complex sample media within the mM range. It should be also considered that optical components of Firesting currently show only limited compatibility with the emission spectrum of the **FI 3** so that simple modification of the emission filter is expected to dramatically (about 10-fold) improve already very good signal-to-noise ratio.

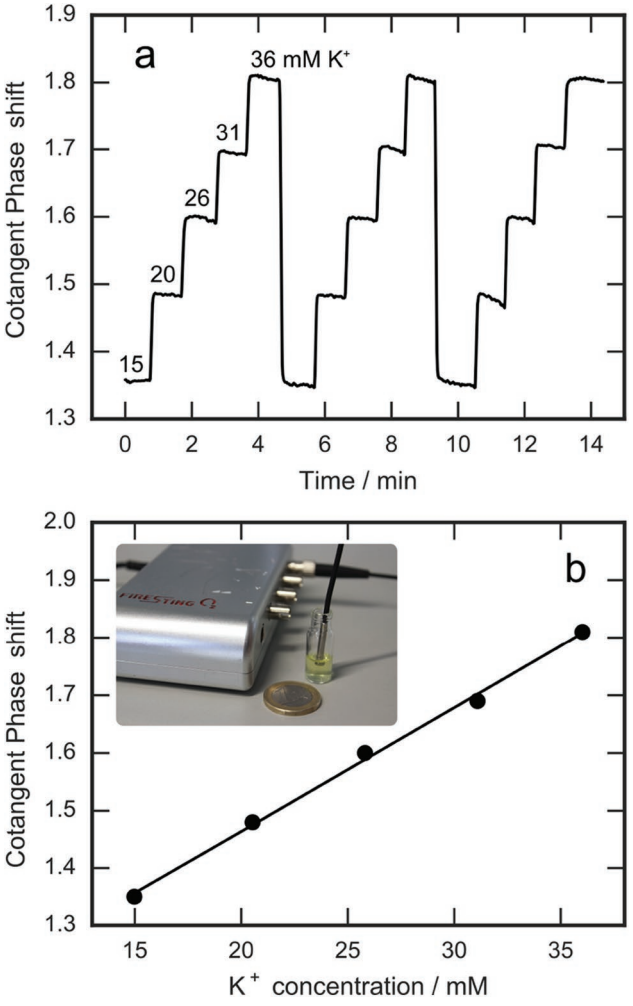

Figure 10. a) Recorded phase shift values of the referenced sensor in FBS samples with different K^+ concentrations. b) Calibration curve of the referenced sensor. The K^+ concentrations were determined using ICP-OES. The inset shows the phase fluorometer (PyroScience Firesting) and an optical plastic fiber with a sensor spot attached to the distal end of the fiber with help of a metal cap.

3. Conclusions

In this contribution we presented a straightforward and efficient strategy leading to optical K^+ sensors with tuneable properties. A palette of new fluoroionophores combines a selective aza-crown receptor and bright and photostable tetraaryl-BODIPY chromophores. Several representatives show absorption and emission in the red/NIR part of the spectrum, high molar absorption coefficients and fluorescence quantum yields. For the first time, the K^+ sensors were obtained by simple immobilization of the fluoroionophores into a stable and biocompatible hydrogel. Despite the simple design, the sensors show no leaching of the indicators, and feature fast and reproducible response. The "off"–"on" enhancement factor can be tuned over a broad range via introduction of electron-donating and electron-withdrawing substituents into the chromophore. The materials show excellent response to K^+ in aqueous solution with a very good selectivity over possible competing ions (e.g., Na^+) and no pH dependency in physiologically relevant conditions. Importantly, the new materials are applicable in a variety of formats, including planar sensor foils and spots, fiber-optic (micro)sensors, and water-dispersible nanosensors and reliably operate even in complex samples such as serum.

DOI: 10.1002/adfm.201603822

The nanoparticles are prepared via a simple procedure and enable extra- and intracellular quantification of potassium. We believe that the above properties of the new high-performance materials will make them valuable analytical tools in biomedical research and diagnostics.

4. Experimental Section

Materials and Methods: ^{1}H NMR spectra were recorded on a 300 MHz instrument from Bruker. MALDI-TOF mass spectra were recorded on a Micromass TofSpec 2E in refectron mode at an accelerating voltage of +20 kV. Absorption measurements were performed on a Cary 50 UV–vis spectrophotometer from Varian. Luminescence spectra, calibrations, quantum yields and lifetimes (TCSPC) were measured on a Fluorolog-3 luminescence spectrometer (Horiba). Calibrations were performed using a peristaltic pump and a home-made flow through cell. Quantum yields were measured using the absolute method in an integrating sphere. QY and lifetimes of the indicators in solution were acquired in THF in presence trifluoroacetic acid (0.3×10^{-3} M) to fully protonate the indicator. QYs for the foils were measured at 1000×10^{-3} M aqueous KCl and 0.1 M aqueous HCl. Leaching was investigated by recording the absorption spectra of a foil during continuous pumping a 100×10^{-3} M KCl solution (20×10^{-3} M TRIS, pH 7.4) through the flow-through cell (10 mL min^{-1}). pKa determination was performed using a 20×10^{-3} M universal buffer (citrate, acetate, BIS-TRIS, and TRIS); pH was adjusted with HCl with help of a digital pH meter (Seven Easy, Mettler Toledo, www.mt.com) calibrated at 25 °C with standard buffers of pH 7.0 and 4.0 (WTW, www.wtw.com). K^+ concentrations of the fetal bovine serum were quantified with an axially viewed ICP-OES (Ciros Vision EOP, Spectro, Germany) using a cross-flow nebulizer, a Scott type spray chamber and a standard ICP torch with a 2.5 mm inner diameter injector. 1200 W RF power, 12 l min^{-1} outer gas flow, 0.7 l min^{-1} intermediate gas flow and 0.83 l min^{-1} nebulizer gas flow were used. K 404.721 nm emission line was used for quantification. Scandium (Sc 361.384 nm) was used as an internal standard at a concentration of 1 mg l^{-1}. Serum measurements with the optode were performed with a Firesting phase fluorometer (www.pyroscience.com) with at a modulation frequency of 4 kHz.

Electrochemical measurements were performed using a VMP3 electrochemical workstation (Biologic). The measurements were carried out at room temperature. A 1 mm diameter gold disc was employed as the working electrodes. A platinum wire served as the counter electrode. Measurements were performed using a Ag/AgCl reference electrode (BAS Inc). Ferrocene was used as reference.

Eudragit RL-100 copolymer (poly-(ethylacrylate-co-methylmethacrylate-co-trimethyl-aminoethyl methacrylate), M.W. ≈ 150 000 Da, 8.8%–12% of quaternary ammonium groups) was from Degussa, Germany (www.evonik.com). Hydrochloric acid 37% (HCl), sodium sulfate anhydrous (Na_2SO_4), and all other solvents including the deuterated solvents were from VWR (www.vwr.com). Polyurethane hydrogel (Hydromed D4) was purchased from AdvanSource biomaterials (www.advbiomaterials.com). Poly(ethylene terephthalate) (PET) support Melinex 505 was obtained from Pütz (www.puetz-folien.com). Poly(styrene-blockvinylpyrrolidone) emulsion in water (38% w/w emulsion in water), lithium diisopropylamide (LDA) (2 M in THF), 2,3-dichloro-5,6-dicyano-p-benzoquinone (DDQ), trifluoracetic acid, Pd(dppf)Cl_2, boron trifluoride etherate (BF_3OEt_2), water-free dichloromethane, and fetal bovine serum were purchased from Aldrich (www.sigmaaldrich.com). 5-Bromo-2-furaldehyde was purchased from ABCR (www.abcr.de). Buffer substances, KCl, NaCl, $CaCl_2$, NH_4Cl, $MgCl_2$ were from Roth (www.carlroth.com). Silica gel (0.04–0.063 mm) was acquired from Acros Organics (www.fishersci.com). Silanized Egyptian blue microparticles (trimethylsilyl form) were prepared according to a literature procedure.[41] All other chemicals were purchased from TCI Europe (www.tcichemicals.com). PMMA fibers (∅ 1 mm) were from Ratioplast (www.ratioplast.com).

Synthesis:N-(4-Formyl-2-Methoxyethoxyphenyl)aza-[18]crown-6 Ether: Synthesis of compound **S3** was performed according to literature procedure[15] and subsequent preparation of compound **S6** was performed according to Ast et at.[16]

3-Phenyl-2H-Azirene: Synthesis was performed according to literature using styrene as starting material.[43]

2-(4-Propylphenyl)-4-Phenylpyrrol (2): 4′-Propylacetophenone (5.00 g, 30.8 mmol, 1 eq) was dissolved in 90 mL dry THF and cooled down to −78 °C. LDA (2 M in THF) (17.05 mL, 1.1 eq) and 3-phenyl-2H-azirene (3.61 g, 30.8 mmol, 1 eq) were added dropwise. The mixture was stirred at −78 °C for 3 h, warmed up to RT, quenched with water and neutralized with diluted HCl. THF was removed under vacuum and the mixture was extracted with DCM, dried over Na_2SO_4 and the solvent removed under vacuum. Purification was performed by column chromatography (silica gel, eluent: CH + DCM = 1 + 1) to obtain the product as white crystals (5.687 g, 18.6%). ^{1}H NMR (300 MHz, CD_2Cl_2) δ 8.49 (bs, 1H), 7.64 – 7.54 (m, 2H), 7.49 – 7.39 (m, 2H), 7.44 – 7.32 (m, 2H), 7.23 (d, J = 7.9 Hz, 3H), 7.16 – 7.08 (m, 1H), 6.87 – 6.79 (m, 1H), 2.63 (t, J = 7.7 Hz, 2H), 1.67 (p, J = 7.4 Hz, 2H), 0.99 (t, J = 7.3 Hz, 3H). DI-EI: m/z: [M$^+$] calcd for $C_{19}H_{19}N$, 261.1518; found, 261.1508.

5-Chloro-3-Phenyl-1,4-Dihydroindeno[1,2-b] Pyrrole (3): The synthesis of **3** was performed analogously to that of **2** but 1.0 g (6.0 mmol) of 5-chloro-1-indanone and 0.70 g (6.0 mmol) of 3-phenyl-2H-azirene were used instead. The product was isolated as white crystals (486 mg, 30%). ^{1}H NMR (300 MHz, CD_2Cl_2) δ 8.56 (bs, 1H), 7.66 – 7.59 (m, 2H), 7.48 (s, 1H), 7.43 – 7.36 (m, 2H), 3.76 (s, 2H). DI-EI: m/z: [MH$^+$] calcd for $C_{17}H_{12}ClN$, 265.0658; found, 265.0656.

4,5-Dihydro-7-Methoxy-3-Phenylbenzo[g]indole (4): The synthesis of **4** was performed analogously to that of **2** but 5.06 g (28.7 mmol) of 6-methoxy-1-tetralone and 3.36 g (28.7 mmol) of 3-phenyl-2H-azirene were used instead. The product was isolated as greenish crystals (2.04 g, 25.8%). ^{1}H NMR (300 MHz, CD_2Cl_2) δ 8.40 (bs, 1H), 7.51 – 7.44 (m, 2H), 7.43 – 7.35 (m, 2H), 7.29 – 7.20 (m, 1H), 7.13 (d, J = 8.4 Hz, 1H), 6.93 (d, J = 2.7 Hz, 1H), 6.84 (s, 1H), 6.76 (dd, J = 8.4, 2.6 Hz, 1H), 3.81 (s, 3H), 2.97 – 2.89 (m, 4H). DI-EI: m/z: [M$^+$] calc for $C_{19}H_{17}NO$, 275.1310; found, 275.1305.

Fluoroionophores: Fluoroionophore FI 1: N-(4-Formyl-2-methoxyethoxyphenyl) aza-[18]crown-6 ether (357 mg, 0.809 mmol, 0.5 eq) and 2,4-dimethylpyrrole (169 mg, 1.78 mmol, 2.2 eq) were dissolved in 5 mL of anhydrous dichloromethane and 1 drop of trifluoroacetic acid was added. The mixture was shielded from light and stirred at RT for 48 h, DDQ (367 mg, 1.61 mmol, 2 eq) was added. After stirring for another 60 min, N,N-diisopropylethylamine (2.15 mL, 12.3 mmol, 15 eq) and BF_3OEt_2 (1.50 mL, 12.3 mmol, 15 eq) were added and stirred for 60 min. The mixture was extracted with water, dried over Na_2SO_4 and the solvent removed in vacuo. The final product was purified by column chromatography and was obtained as purple crystals (117 mg, 22%). UV–vis (DCM): λ_{max} (ε), nm (M^{-1} cm^{-1}) = 504 (53600). ^{1}H NMR (300 MHz, $CDCl_3$) δ 7.25 (m, 1H), 7.06 – 6.82 (m, 2H), 6.00 (s, 2H), 4.35 – 4.14 (m, 2H), 3.80 – 3.23 (m, 29H), 2.55 (s, 6H), 1.47 (s, 6H). MALDI-TOF: m/z: [MH$^+$] calcd for $C_{34}H_{49}N_3O_7$, 660.364; found, 660.389.

Fluoroionophore FI 2: The synthesis of **FI 2** was performed analogously to that of **FI 1** but 100 mg (0.226 mmol) of N-(4-formyl-2-methoxyethoxyphenyl) aza-[18]crown-6 ether and 120 mg (0.459 mmol) of 2-(4-propylphenyl)-4-phenylpyrrole were used instead. The product was isolated as purple crystals (58 mg, 26%). UV–vis (DCM): λ_{max} (ε), nm (M^{-1} cm^{-1}) = 571 (29900). ^{1}H NMR (300 MHz, CD_2Cl_2) δ 7.68 (d, J = 7.8 Hz, 4H), 7.21 (d, J = 7.9 Hz, 4H), 6.91 – 6.81 (m, 10H), 6.49 (s, 2H), 3.65 – 3.27 (m, 31H), 2.62 – 2.54 (m, 4H), 1.66 – 1.58 (m, 4H), 0.91 (t, J = 7.3 Hz, 6H). MALDI-TOF: m/z: [MK$^+$] calcd for $C_{60}H_{68}BF_2N_3O_7K$, 1030.4766; found, 1030.4915.

Fluoroionophore FI 3: The synthesis of **FI 3** was performed analogously to that of FI 1 but 256 mg (0.582 mmol) of N-(4-formyl-2-methoxyethoxyphenyl) aza-[18]crown-6 ether and 299 mg (1.164 mmol) of 5-chloro-3-phenyl-1,4-dihydroindeno[1,2-b]pyrrole were used instead. The product was isolated as green crystals (125 mg, 21%). UV–vis (DCM): λ_{max} (ε), nm (M^{-1} cm^{-1}) = 640 (109300), 589 (20000). ^{1}H NMR (300 MHz, CD_2Cl_2) δ 8.32 (d, J = 8.3 Hz, 2H), 7.52 (d, J = 7.1 Hz, 4H), 7.06 – 6.85 (m, 10H), 6.75 – 6.57 (m, 2H), 6.47 – 6.29 (m, 1H),

3.78 – 3.34 (m, 31H), 1.27 (s, 4H). MALDI-TOF: m/z: [MH^+] calcd for $C_{56}H_{55}BF_2Cl_2N_3O_7$, 1000.3488; found, 1000.3410.

Fluoroionophore FI 4: The synthesis of **FI 4** was performed analogously to that of **FI 1** but 100 mg (0.226 mmol) of N-(4-formyl-2-methoxyethoxyphenyl) aza-[18]crown-6 ether and 124 mg (0.452 mmol) of 4,5-dihydro-7-methoxy-3-phenylbenzo[g]indole were used instead. The product was isolated as green crystals (41 mg, 18%). UV–vis (DCM): λ_{max} (ε), nm ($M^{-1}cm^{-1}$) = 655 (87200), 601 (22000). ^{1}H NMR (300 MHz, CD_2Cl_2) δ 8.74 (d, J = 8.9 Hz, 2H), 7.11 – 6.70 (m, 17H), 3.89 (s, 6H), 3.73 – 3.34 (m, 31H), 2.91 – 2.68 (m, 4H), 2.44 – 2.32 (m, 4H). MALDI-TOF: m/z: [MNa^+] calcd for $C_{60}H_{65}BF_2N_3O_9Na$, 1020.4792; found, 1020.4977.

5-(3-Chloro-4-Methoxyphenyl)-Furan-2-Carbaldehyde (5): 5-Bromo-2-furaldehyde (3.00 g, 0.017 mol, 1 eq), 3-chloro-4-methoxyphenyl) boronic acid (3.20 g, 0.017 mol, 1 eq) and Na_2CO_3 (60 mL of 2 M solution) and) were dissolved in 300 mL toluene and 60 mL ethanol. The mixture was degassed for 20 min by vigorously stirring under heavy Ar flow. After addition of the catalyst [1,1′-bis(diphenylphosphino) ferrocene] dichloropalladium(II) ($Pd(dppf)Cl_2$) (20.0 mg, 0.15 mol%) the reaction mixture was heated up to 80 °C and stirred for 18 h under inert atmosphere. After cooling, the organic phase was washed with water and brine, dried over Na_2SO_4 and evaporated. The resulting residue was purified by column chromatography (silica gel, eluent: CH + DCM = 1 + 1 to 1 + 5) to obtain 5-(4-methoxyphenyl)-furan-2-carbaldehyde as a yellow solid (2.89 g, 71.1%). ^{1}H NMR (300 MHz, $CDCl_3$) δ 9.63 (s, 1H), 7.84 (d, J = 2.2 Hz, 1H), 7.71 (dd, J = 8.6, 2.2 Hz, 1H), 7.31 (d, J = 3.7 Hz, 1H), 6.99 (d, J = 8.6 Hz, 1H), 6.74 (d, J = 3.7 Hz, 1H), 3.96 (s, 3H).

Ethyl-2-Azidoacetate (6): Ethyl 2-bromoacetate (11.50 mL, 0.10 mol, 1 eq) and NaN_3 (13.20 g, 0.20 mol, 2 eq) were stirred in 300 mL acetone and 100 mL H_2O. After 1 h the reaction solution was extracted with DCM and brine (3×), the organic phase dried with Na_2SO_4 and concentrated under vacuum and yields in a colorless liquid (12.53 g, 93.9%). ^{1}H NMR (300 MHz, $CDCl_3$) δ 4.27 (q, J = 7.1 Hz, 2H), 3.87 (s, 2H), 1.32 (t, J = 7.1 Hz, 3H).

2-(3-Chloro-4-Methoxyphenyl)-4H-furo[3,2-b] Pyrrole-5-Carboxylic Acid Ethyl Ester (7): 5-(3-Chloro-4-methoxyphenyl)-furan-2-carbaldehyde (2.02 g, 8.54 mmol, 1 eq) and ethyl 2-azidoacetate (4.0 mL, 34.7 mmol, 4 eq) were dissolved in 120 mL anhydrous ethanol and cooled down to 0 °C. Sodium ethoxide (20 w% in ethanol, 25 mL, 34.7 mmol, 4 eq) was added dropwise over 30 min and stirred for 3 h. The reaction mixture was poured on 250 mL sat. NH_4Cl solution, the precipitate collected and washed with H_2O. The intermediate product was dissolved in 85 mL toluene, refluxed for 4 h. A precipitation forms after cooling down to RT and the solvent was removed using rotary evaporator. Column chromatography (silica gel, eluent: CH + EE = 5 + 1 to 1 + 1) was performed and the product was obtained as an orange solid (1.44 g, 52.7%). ^{1}H NMR (300 MHz, $CDCl_3$) δ 8.86 (bs, 1H), 7.73 (s, 1H), 7.58 (d, J = 8.6 Hz, 1H), 6.95 (d, J = 8.7 Hz, 1H), 6.79 (s, 1H), 6.59 (s, 1H), 4.36 (q, J = 7.1 Hz, 2H), 3.93 (s, 3H), 1.39 (t, J = 7.2 Hz, 3H). DI-EI: m/z: [M^+] calcd for $C_{16}H_{14}NO_4Cl$, 319.0611; found, 319.0599.

2-(3-Chloro-4-Methoxyphenyl)-4H-furo[3,2-b] Pyrrole-5-Carboxylic Acid (8): 2-(3-Chloro-4-methoxyphenyl)-4H-furo[3,2-b] pyrrole-5-carboxylic acid ethyl ester (780 mg, 2.44 mmol, 1 eq) was dissolved in 25 mL ethanol and a NaOH (7 mL of 2.5 M solution) was added and the mixture was refluxed for 1 h. After cooling, HCl conc. was added resulting in a green precipitate. The resulting precipitate was filtered and washed with H_2O and dried in the oven at 60 °C overnight (548 .7 mg, 70%). 1H NMR (300 MHz, DMSO-d6) δ 11.60 (bs, 1H), 7.87 (d, J = 2.2 Hz, 1H), 7.74 (dd, J = 8.7, 2.2 Hz, 1H), 7.21 (d, J = 8.7 Hz, 1H), 7.11 (s, 1H), 6.71 (s, 1H), 3.89 (s, 3H). DI-EI: m/z: [M+] calcd for $C_{14}H_{10}NO_4Cl$, 291.0298; found, 291.0299.

Fluoroionophore FI 5: 2-(3-Chloro-4-methoxyphenyl)-4H-furo[3,2-b] pyrrole-5-carboxylic acid (127.9 mg, 0,438 mmol, 1 eq) and N-(4-formyl-2-methoxyethoxyphenyl) aza-[18]crown-6 ether (96.2 mg, 0.218 mmol, 0.5 eq) were dissolved in 3 mL conc. trifluoroacetic acid under Ar atmosphere. The mixture was stirred at 50 °C for 1 h, $POCl_3$ (0.50 mL) was added, the stirred for 10 min at 50 °C and precipitated slowly into cold water. The precipitate was collected and transferred into a Schlenk tube and dried via vacuum and 5 mL water-free DCM was added under an Ar atmosphere. N,N-Diisopropylethylamine (305 µL, 1.75 mmol, 4 eq) and BF_3OEt_2 (220 µL, 1.75 mmol, 4 eq) were added to the solution and after 60 min stirring, the solution was extracted with H_2O, dried over Na_2SO_4 and concentrated under vacuum. The crude product was purified using column chromatography (silica gel, eluent: DCM + MeOH = 100 + 1 to 100 + 20) to obtain the dye as green blue crystals (35 mg, 8.3%). UV–vis (DCM): λ_{max} (ε), nm (M^{-1} cm^{-1}) = 670 (195600), 616 (48500). ^{1}H NMR (300 MHz, $CDCl_3$) δ 7.80 (d, J = 2.2 Hz, 2H), 7.66 (dd, J = 8.6, 2.2 Hz, 2H), 7.16 (d, J = 4.8 Hz, 2H), 6.98 (d, J = 8.8 Hz, 2H), 6.87 (s, 2H), 6.34 (s, 2H), 4.22 (s, 2H), 3.94 (s, 6H), 3.82 – 3.49 (m, 26H), 3.43 (s, 3H). MALDI-TOF: m/z: [MNa^+] calcd for $C_{48}H_{50}BCl_2F_2N_3O_{11}Na$, 986.2789; found, 986.4067.

Planar Sensor Films: An appropriate amount of the indicator was dissolved in a hydrogel D4 stock solution (10 wt% in THF). Sensor films were prepared by knife coating of these "sensor cocktails" onto dust-free PET foils (25 µm wet film thickness). Dye concentrations for calibrations and QY determination were 0.2 wt% and for leaching experiment 1 wt% in respect to the polymer.

Fiber-Optic Sensor: 0.5 mg **FI 3**, 20 mg of silanized Egyptian blue and 100 mg hydrogel D4 were dissolved in 1 g THF. The "cocktail" was knife coated onto a dust-free PET foil (75 µm wet film thickness). A sensor spot (≈2 mm diameter) was stamped out and fixed with a metal cap on a 1 m PMMA fiber.

RL100 Particles: 100 mg Eudragit RL100 were dissolved in 50 mL acetone, and indicator dye **FI 3** (1 mg) was added. 250 mL water was added quickly under vigorous stirring (3 s); acetone was removed using rotary evaporator and the particle dispersion was further concentrated to a volume of 50 mL. For calibrations 0.5 mL of particle dispersion were added to 2 mL of KCl aqueous solutions.

PS/PVP Particles: 213 mg of the PS/PVP emulsion (38% emulsion in water) was diluted with 25 mL H_2O and 20 mL EtOH. **FI 3** (1 mg, 1 wt%) was dissolved in 20 mL EtOH and was added dropwise under vigorous stirring into the emulsion of the polymer. The emulsion was concentrated under reduced pressure to remove all ethanol and partly water. It was then diluted with water up to 10 mL overall volume. For calibration 20 µL of the solution were added to 1980 µL buffered KCl solution.

Supporting Information

Supporting Information is available from the Wiley Online Library or from the author.

Acknowledgements

The authors would like to thank Georg Michelitsch, Bianca Hörler, Josef Lechner, Nicole Steinmann, and Lukas Heupl for support in synthesis of the indicators and receptors. The authors gratefully acknowledge Stefan Freudenberger and Nika Mahne from the Institute for Chemistry and Technology of Materials (TU Graz) for the help with the cyclovoltametry measurements. Helmar Wiltsche and Monika Winkler of the Institute of Analytical Chemistry and Food Chemistry (TU Graz) are thanked for the help with the ICP-OES measurements. Financial support from European Commission ("Schema" Project No. 614002) is gratefully acknowledged.

Received: July 27, 2016
Published online:

[1] J. M. Burnell, B. H. Scribner, B. T. Uyeno, M. F. Villamil, *J. Clin. Invest.* **1956**, *35*, 935.
[2] J. R. Elkinton, A. W. Winkler, *J. Clin. Invest.* **1944**, *23*, 93.
[3] B. Hille, *Prog. Biophys. Mol. Biol.* **1970**, *21*, 1.

[4] H. Eagle, *Science* **1955**, *122*, 501.
[5] P. K. Whelton, J. He, J. A. Cutler, F. L. Brancati, L. J. Appel, D. Follmann, M. J. Klag, *JAMA* **1997**, *277*, 1624.
[6] D. C. Gadsby, R. Niedergerke, S. Page, *Nature* **1971**, *232*, 651.
[7] A. L. Hodgkin, *Biol. Rev.* **1951**, *26*, 339.
[8] M. Näbauer, S. Kääb, *Cardiovasc. Res.* **1998**, *37*, 324.
[9] J. K. Tusa, H. He, *J. Mater. Chem.* **2005**, *15*, 2640.
[10] T. L. Doane, C. Burda, *Chem. Soc. Rev.* **2012**, *41*, 2885.
[11] M. Schäferling, *Angew. Chem. Int. Ed.* **2012**, *51*, 3532.
[12] M. J. Ruedas-Rama, J. D. Walters, A. Orte, E. A. H. Hall, *Anal. Chim. Acta* **2012**, *751*, 1.
[13] A. P. de Silva, T. S. Moody, G. D. Wright, *Analyst* **2009**, *134*, 2385.
[14] K. Meuwis, N. Boens, F. C. De Schryver, J. Gallay, M. Vincent, *Biophys. J.* **1995**, *68*, 2469.
[15] H. He, M. A. Mortellaro, M. J. P. Leiner, R. J. Fraatz, J. K. Tusa, *J. Am. Chem. Soc.* **2003**, *125*, 1468.
[16] S. Ast, T. Schwarze, H. Müller, A. Sukhanov, S. Michaelis, J. Wegener, O. S. Wolfbeis, T. Körzdörfer, A. Dürkop, H.-J. Holdt, *Chem. Eur. J.* **2013**, *19*, 14911.
[17] R. D. Carpenter, A. S. Verkman, *Eur. J. Org. Chem.* **2011**, *2011*, 1242.
[18] M. Magzoub, P. Padmawar, J. A. Dix, A. S. Verkman, *J. Phys. Chem. B* **2006**, *110*, 21216.
[19] P. Padmawar, X. Yao, O. Bloch, G. T. Manley, A. S. Verkman, *Nat. Methods* **2005**, *2*, 825.
[20] X. Zhou, F. Su, W. Gao, Y. Tian, C. Youngbull, R. H. Johnson, D. R. Meldrum, *Biomaterials* **2011**, *32*, 8574.
[21] X. Kong, F. Su, L. Zhang, J. Yaron, F. Lee, Z. Shi, Y. Tian, D. R. Meldrum, *Angew. Chem. Int. Ed.* **2015**, *54*, 12053.
[22] T. Hirata, T. Terai, T. Komatsu, K. Hanaoka, T. Nagano, *Bioorg. Med. Chem. Lett.* **2011**, *21*, 6090.
[23] B. Sui, X. Yue, M. G. Tichy, T. Liu, K. D. Belfield, *Eur. J. Org. Chem.* **2015**, *2015*, 1189.
[24] J.-P. Malval, I. Leray, B. Valeur, *New J. Chem.* **2005**, *29*, 1089.
[25] M. Baruah, W. Qin, R. A. L. Vallée, D. Beljonne, T. Rohand, W. Dehaen, N. Boens, *Org. Lett.* **2005**, *7*, 4377.
[26] W. Namkung, P. Padmawar, A. D. Mills, A. S. Verkman, *J. Am. Chem. Soc.* **2008**, *130*, 7794.
[27] X. Zhou, F. Su, Y. Tian, C. Youngbull, R. H. Johnson, D. R. Meldrum, *J. Am. Chem. Soc.* **2011**, *133*, 18530.
[28] W. Zhao, E. M. Carreira, *Chem. Eur. J.* **2006**, *12*, 7254.
[29] S. K. Yang, X. Shi, S. Park, T. Ha, S. C. Zimmerman, *Nat. Chem.* **2013**, *5*, 692.
[30] K. Umezawa, Y. Nakamura, H. Makino, D. Citterio, K. Suzuki, *J. Am. Chem. Soc.* **2008**, *130*, 1550.
[31] N. Boens, V. Leen, W. Dehaen, *Chem. Soc. Rev.* **2012**, *41*, 1130.
[32] A. Weller, *Pure Appl. Chem.* **1968**, *16*, 125.
[33] C. Deutsch, J. S. Taylor, D. F. Wilson, *Proc. Natl. Acad. Sci. USA* **1982**, *79*, 7944.
[34] D. Aigner, S. M. Borisov, P. Petritsch, I. Klimant, *Chem. Commun.* **2013**, *49*, 2139.
[35] A. Fercher, S. M. Borisov, A. V. Zhdanov, I. Klimant, D. B. Papkovsky, *ACS Nano* **2011**, *5*, 5499.
[36] S. Das, P. K. Suresh, R. Desmukh, *Nanomed. Nanotechnol. Biol. Med.* **2010**, *6*, 318.
[37] U. K. Sharma, A. Verma, S. K. Prajapati, H. Pandey, A. C. Pandey, *Appl. Nanosci.* **2014**, *5*, 143.
[38] K. Dillen, J. Vandervoort, G. Van den Mooter, A. Ludwig, *Int. J. Pharm.* **2006**, *314*, 72.
[39] S. M. Borisov, T. Mayr, G. Mistlberger, K. Waich, K. Koren, P. Chojnacki, I. Klimant, *Talanta* **2009**, *79*, 1322.
[40] S. M. Borisov, T. Mayr, I. Klimant, *Anal. Chem.* **2008**, *80*, 573.
[41] S. M. Borisov, C. Würth, U. Resch-Genger, I. Klimant, *Anal. Chem.* **2013**, *85*, 9371.
[42] I. Klimant, C. Huber, G. Liebsch, G. Neurauter, A. Stangelmayer, O. S. Wolfbeis, in *New Trends in Fluorescence Spectroscopy*, Springer Series on Fluorescence (Eds: P. B. Valeur, D. J.-C. Brochon), Springer, Berlin **2001**, pp. 257–274.
[43] A. G. Hortmann, D. A. Robertson, B. K. Gillard, *J. Org. Chem.* **1972**, *37*, 322.